A Series of Cation-Modified Robust Zirconium-Based Metal-Organic Frameworks for Carbon Dioxide Capture

Guoyu Zhang [a], Feng Xie [a], Thomas M. Osborn Popp [a], Akash Patel [a], Eder Moisés Cedeño Morales [b], Kui Tan [b], Ryan Crichton [a], Gene Hall [a], Jianyuan Zhang [a], Andrew J. Nieuwkoop [a], and Jing Li [a,]*

[a] Department of Chemistry and Chemical Biology, Rutgers University, 123 Bevier Road,
Piscataway, New Jersey 08854, USA
[b] Department of Materials Science and Engineering, University of Texas at Dallas, 800 West
Campbell Road, Richardson, Texas, 75080, USA

Abstract: Metal-organic frameworks (MOFs) represent one of the most promising porous solids for possible use as sorbents to control and reduce the greenhouse gas emission. Studies have shown that open metal sites (OMS) interact strongly with carbon dioxide and thus, serve as efficient binding sites for CO_2 capture. However, many OMS-bearing MOFs are lack of framework stability and often have high regeneration temperature. To seek ways to solve the stability issue, we designed a series of isoreticular MOFs, Zr-tcpb-COOM (M = alkali/alkaline earth metal), by exchange of metal ions with protons on Zr-tcpb-COOH via post-synthetic modifications (PSM). The pristine MOF (Zr-tcpb-COOH) has a very robust framework. The PSM process does not deteriorate the framework stability but creates metal binding sites that form strong bonds with carbon dioxide. The results show that at low CO_2 pressure, the uptake amount is enhanced considerably using Zr-tcpb-COOM and is in trend of increasing atomic number ($Li^+ < Na^+ < K^+ < Ca^{2+}$). High adsorption selectivity (CO_2/N_2 IAST selectivity (15:85) = 539.5) is also achieved for CO_2 over N_2 at room temperature. This approach offers a feasible method to improve CO_2 capture capacity, especially at low concentrations.

Keywords: Metal-organic framework, Adsorbent, CO_2 capture, Post-synthetic modification, Alkali and alkaline metal binding sit

---

1. Introduction

Due to the booming industrialization and population increase in the last century, the emission of greenhouse gases has become an inevitable problem.[1, 2] Climate change, largely induced by the rapid increase of such emissions, is a major challenge of our era.[3] History will look back at this period and reflect on what contributions scientists have made. Besides relying on developing renewable clean energy and improving the energy efficiency of current technologies, negative emissions technologies (NETs) are the answer to this historical strait.[4, 5] Traditional NET mainly utilizes amine/inorganic based aqueous solutions to adsorb CO_2 and dispose carbamate or bicarbonate forms of CO_2 from the solution phase. However, this technology faces several drawbacks such as significant energy input for regeneration due to large heat capacity, bulky volume occupancy, high corrosion, and degradation.[6, 7] Its replacement by more advanced technologies is urgently demanded globally.

Adsorption based technologies using highly porous solids have been considered as the next generation of NETs because of the large capacity, high selectivity, and relatively low regeneration energy associated with these technologies.[8] Metal-organic frameworks (MOFs) are one of the most promising candidates among the known sorbents, not only because they have all the desired features mentioned above, but also because they possess unbeatable tunability and functionality.[9-13] Although high adsorption capacity for CO_2 has been achieved by MOFs, many of them only perform well at higher pressure/concentration; Others that do take up sufficiently high amount of CO_2 at low concentrations (e.g., in ambient air, ~400 ppm) are usually via chemisorption. The easy functionalization of MOFs allows creation of strong CO_2-MOF interaction sites to selectively capture CO_2 over other abundant gases such as N_2, O_2, CH_4 etc.[1, 10] Thus far, MOFs with four types of binding sites have been largely used for the selective chemisorption of CO_2: 1) Amine-appended sites;[14-18] 2) M-OH active sites (M = Zn, Co, Ni, Mn); [19-21] 3) NH_2 functionalized sites of ligands;[22-24] and 4) OMS, [25-29] all of which have shown good performance regarding capacity and selectivity. However, MOFs in the first two groups suffer consistently from the loss of active sites after long-term usage and thus, have low recyclability.[7, 30] The third method requires extra steps in ligand synthesis and sometimes suffers from amine oxidation, resulting in high cost. Comparably, the creation of OMS (the fourth method) is a straightforward and effective way to boost CO_2 affinity and enhance the uptake amount significantly at low concentrations. However, often MOFs with OMS are water/moisture sensitive and can't be sustained under ambient conditions for long period of time. In addition, if generation of OMS must be done by heating (in cases where solvent exchange are unsuccessful) the temperature required to remove the coordinated solvents with high boiling points (e.g., DMF & DMA) will be rather high, which may cause structure collapse.[31, 32] To address these issues, we have attempted to embed reactive metal sites into a robust MOF that does not have OMS via post-synthetic modification (PSM) process. This approach also allows us to introduce different metal ions into the same structure by the same method to tune the CO_2 capture performance. Only a few papers using similar approach have been reported[33-35] for CO_2 capture and none of them have carried out a systematic study to compare the performance of different metal cations.

Herein, we report the synthesis of a 4,8-connected zirconium-based metal-organic framework Zr-tcpb-COOH made of a hexacarboxylate ligand (1,2,4,5-tetrakis(4-carboxyphenyl)-3,6-dicarboxyl-benzene, H_4tcpb-$(COOH)_2$) and its cation exchanged form, Zr-tcpb-COOM (M = Li, Na, K, and Ca) by PSM process. The original structure Zr-tcpb-COOH, which contains two free, non-coordinated carboxylic groups, is isoreticular to Zr-tcpb (CAU-24).[36] The unbonded carboxylic acid groups in Zr-tcpb-COOH can react readily with M^+/M^{2+} in basic alkali/alkaline solutions through acid-base neutralization to form Zr-tcpb-COOM, which are then used to evaluate the CO_2 adsorption performance. The results reveal that at the low concentration of CO_2, the uptake amounts of these metal cation embedded Zr-tcpb-COOM MOFs show obvious enhancement, and the uptake capacity increases as a function of increasing atom number of the metal cations (Li^+ < Na^+ < K^+ < Ca^{2+}). Furthermore, the Zr-tcpb-COOM MOFs exhibit high moisture and chemical stability, thermal stability, and recyclability.

2. Experimental Section

2.1 General Information

All reagents are used as purchased unless specified otherwise. Detailed information about the sources of chemicals is provided in the Supporting Information.

2.2 Synthesis of ligand H_4tcpb-$(COOH)_2$

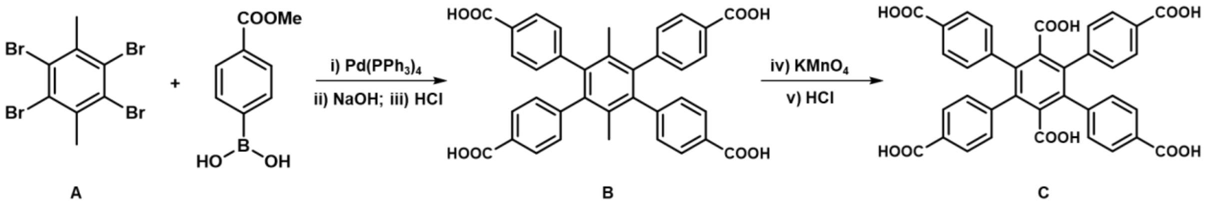

Scheme 1. Synthesis of 1,2,4,5-tetrakis(4-carboxyphenyl)-3,6-dicarboxyl-benzene (H_4tcpb-$(COOH)_2$)

The hexacarboxylic acid 1,2,4,5-tetrakis(4-carboxyphenyl)-3,6-dicarboxyl-benzene (H_4tcpb-$(COOH)_2$) was synthesized through the Suzuki coupling reactions and subsequent oxidation. In a 500 mL three-necked round bottom flask, 1,2,4,5-tetrabromo-3,6-dimethyl-benzene (A) (2.1 g, 5 mmol), 4-methoxycarbonylphenylboronic acid (5.4 g, 30 mmol), K_3PO_4 (6.36 g, 30 mmol), and $Pd(PPh_3)_4$ (0.578 g, 0.5 mmol) were mixed in degassed 1,4-dioxane (200 mL). The mixture was heated at 90 °C under nitrogen atmosphere for 3 days. The reaction was monitored by TLC. After the starting materials disappeared, the organic solvent was then removed under reduced pressure and 120 mL of water was added to the solid residual which was extracted by dichloromethane (3 × 60 mL). The organic phases were combined, washed with brine, and dried over $MgSO_4$ overnight. The organic solvent was removed by rotary evaporation to give the crude product which was purified by column chromatography (Eluent: Hexane/Ethyl acetate = 4:1). The obtained ester was then hydrolyzed in a mixture of NaOH aqueous solution (6M, 50 mL), tetrahydrofuran (50 mL), and methanol (50 mL) by reflux overnight to give the pure form of compound B, 1,2,4,5-tetrakis(4-carboxyphenyl)-3,6-dimethyl-benzene (H_4tcpb-$(Me)_2$). (2.1 g, Yield: 73%). ^1H NMR (500 MHz, DMSO-d6, δ): 1.64 (s, 6H, CH_3), 7.19 (d, 8H, Ar H), 7.72 (d, 8H, Ar H), 12.87 (s, 4H, COOH).

In a 250 mL round bottom flask, compound B (2 g, 3.4 mmol) was dissolved in a mixture of NaOH aqueous solution (2M, 100 mL) and tBuOH (30 mL). Then, 6 g of $KMnO_4$ was slowly added to the solution over 3 days (2 g each day) at 80 °C. After the color of the $KMnO_4$ solution faded, the clear filtrate was obtained via reducing pressure filtration. The final product of compound C could be precipitated out by acidifying the solution with 6M HCl aqueous solution and was further dried in the vacuum oven at 80 °C overnight (1.8 g, Yield: 89%). ^1H NMR (500 MHz, DMSO-d6, δ): 7.26 (d, 8H, Ar H), 7.70 (d, 8H, Ar H), 12.91 (s, 6H, COOH). Peaks of compound B and C are assigned and integrated to confirm the structure (Figure S1 and Figure S2).

2.3 Synthesis of Zr-tcpb, Zr-tcpb-Me and Zr-tcpb-COOH

Synthesis of Zr-tcpb. Zr-tcpb was synthesized via a solvothermal reaction according to the previous procedure (CAU-24).[36] $ZrOCl_2·8H_2O$ (85 mg, 0.26 mmol) and H_4tcpb (29.8 mg, 0.05 mmol) was dispersed in a mixture of DMF (3 mL) and formic acid (1 mL) solution in a 20 mL glass vial. The mixture was then sonicated for 30 minutes. The vial was capped tightly and put into a pre-heated 120 °C oven overnight. The white crystalline precipitate was filtrated and washed with fresh DMF and MeOH several times. The product was characterized by PXRD.

Synthesis of Zr-tcpb-Me. Zr-tcpb-Me was synthesized via a solvothermal reaction. $ZrOCl_2·8H_2O$ (85 mg, 0.26 mmol) and H_4tcpb-$(Me)_2$ (31.23 mg, 0.05 mmol) was added to a mixture of DMF (3 mL) and formic acid (1.5 mL) solution in a 20 ml glass vial. The mixture was then sonicated for 30 minutes. The vial was capped tightly and put into a pre-heated 120 °C oven overnight. The white precipitate was obtained after filtration and washing with fresh DMF and MeOH several times. The product was characterized by PXRD.

Synthesis of Zr-tcpb-COOH. Zr-tcpb-COOH was synthesized via a solvothermal reaction. $ZrOCl_2·8H_2O$ (42.5 mg, 0.13 mmol) and H_4tcpb-$(COOH)_2$ (17.3 mg, 0.025 mmol) was added to a mixture of DMA (4 mL) and formic acid (2 mL) solution in a 20 ml glass vial. The mixture was then sonicated for 30 minutes. The vial was capped tightly and put into a pre-heated 120 °C oven for 3 days. The white precipitate was obtained after filtration and washing with fresh DMA and MeOH several times. The product was characterized by PXRD.

2.4 Post-synthetic Modification of Zr-tcpb-COOH

As-made Zr-tcpb-COOH samples (100 mg each) were soaked in 20 mL of fresh MeOH and kept at room temperature overnight. The sample was then filtered and immersed into corresponding 0.01 M aqueous alkali/alkaline solutions (LiOH, NaOH, KOH, and $Ca(OH)_2$) and stirred at 40 °C overnight. The base-treated samples were filtered and washed with 3 × 10 mL of DI water and 2 × 10 mL of MeOH. The presence of alkali/alkaline cation was analyzed and confirmed by solid-state NMR (ss-NMR), X-ray fluorescence (XRF) and X-ray photoelectron spectroscopy (XPS) measurement.

2.5 Gas Adsorption Measurements

Gas adsorption measurements were carried out on a Micromeritics 3Flex volumetric adsorption analyzer. Liquid nitrogen and a circulating-bath with digital temperature controller were used for measurements at 77 K and temperatures near room temperature, respectively. For each adsorption measurement, around 80 mg as-synthesized sample was used and activated at 100 °C under dynamic vacuum for 6 hours prior to adsorption experiments.

The single-component isotherms for CO_2 recyclability experiment and H_2O adsorption were collected in a gravimetric adsorption analyzer TGA Q50 (TA Instruments). For water adsorption experiments, pure N_2 gas was purged through the bubbler containing water and was performed as the carrier gas of saturated water vapor. The partial pressure of CO_2 or H_2O was adjusted by controlling the ratio of pure N_2 gas and CO_2 or saturated water vapor. Approximately 20 mg of samples was activated under a constant N_2 flow for 30 mins at 373 K. Adsorbed amounts were monitored by weight changes in the sample and continuously monitored throughout the experiments.

2.6 Solid-State NMR Experiments

Solid state NMR spectra were acquired at 9.4 T using a Bruker Avance III spectrometer equipped with a Bruker 3.2 mm HXY probe, using a frequency of 400.2 MHz for ^{1}H, 155.5 MHz for ^{7}Li, 105.9 MHz for ^{23}Na, and 100.6 MHz for ^{13}C. All spectra were acquired at 20 °C and 20 kHz MAS. ^{13}C cross polarization (CP) MAS experiments were acquired using a 5 ms contact period, 2 s inter-scan delay, and 100 kHz TPPM ^{1}H decoupling during acquisition. ^{1}H, ^{7}Li, and ^{23}Na spectra were collected using a $\pi/2$ pulse-acquire sequence, with inter-scan delays set to approximately $5*T_1$ at

2 s, 3 s, and 0.5 s for ^{1}H, ^{7}Li, and ^{23}Na respectively. Chemical shifts were referenced to the downfield ^{13}C resonance of adamantane at 38.48 ppm.

2.7 FT-IR Measurement

IR measurements were performed on a Nicolet 6700 FTIR spectrometer equipped with a liquid N_2-cooled mercury cadmium telluride MCT-A detector. The sample of MOF compound (Zr-tcpb-COOH, Zr-tcpb-COOLi, Zr-tcpb-COONa, and Zr-tcpb-COOK) (~2 mg each) was pressed onto a KBr pellet and placed into a vacuum cell placed at the focal point of the sample compartment of the infrared spectrometer. The cell was connected to a vacuum line for evacuation. All spectra were recorded under vacuum (base pressure < 20 mTorr) in transmission mode with a frequency range of 600−4000 cm−1 (4 cm−1 spectral resolution).

3. Results and Discussion

It is well known that one of the most stable MOF families are zirconium-based compounds built on Zr_6 hexanuclear clusters (Figure 1a) with a maximum 12-connectivity. They also feature well-controlled synthesis, easy reproducibility and rich structural tunability.[37] In general, it is straightforward to obtain isoreticular structures with the same topology, simply by functionalizing the parent ligands,[38] for example, adding small functional groups without changing their overall length and connectivity. Therefore, taking the parent structure of Zr-tcpb (CAU-24)[36], we functionalized ligand by adding methyl group and carboxylic group to the central benzene ring. The MOF synthesis conditions with the modified ligands were adjusted and two isoreticular MOFs Zr-tcpb-Me and Zr-tcpb-COOH were successfully synthesized under solvothermal reactions. Two free carboxylic acid groups added to the ligands were not bonded to the zirconium clusters and will thus be available as binding sites for alkali/alkaline metal ions via PSM procedure (Figure 1b). The powder X-ray diffraction (PXRD) patterns of the as-made samples of Zr-tcpb-Me and Zr-tcpb-COOH match well with the as-made sample of Zr-tcpb as well as the simulated pattern (Figure 2a), confirming that the ligand functionalized structures are isoreticular to the parent structure. We also obtained simulated structure of Zr-tcpb-COOH using crystal builder and material visualizer modules of *Material Studio 7* (Figure 1c). Like the parent structure, it crystallizes in a C-centered orthorhombic system with space group *Cmmm* and features a 4,8-connected **scu** topology. The structure contains 1D open channels along both the *a*-axis and *c*-axis. While the channels along the *a*-axis may be too small, those along the *c*-axis are more than enough to accommodate metal cations at the free -COOH sites. All three isoreticular MOFs, Zr-tcpb, Zr-tcpb-Me and Zr-tcpb-COOH exhibit high thermal stability. Thermogravimetric (TG) analysis show that their decomposition temperatures are above 400 °C (Figure 2c).

3.1 Synthesis and Structure Characterization

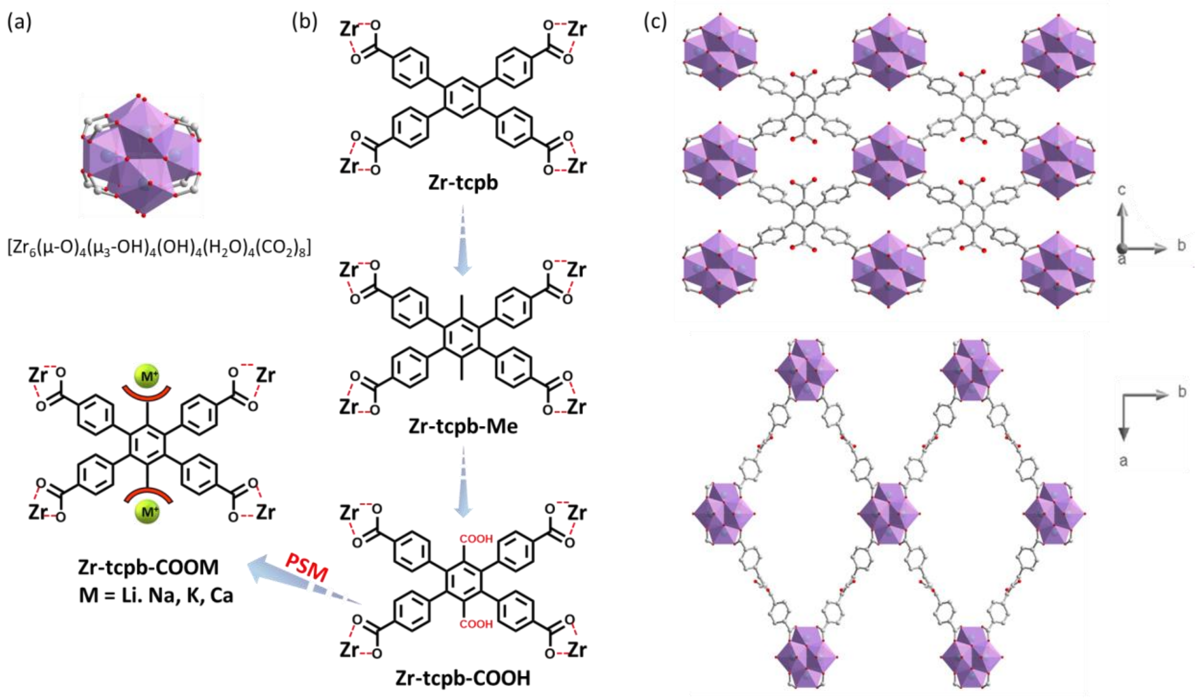

Figure 1. (a) The hexanuclear 8-connected Zr_6 cluster; (b) The experimental design of Zr-tcpb-X series through ligand functionalization and post-synthetic modification (PSM) for CO_2 capture; (c) Simulated structure of Zr-tcpb-COOH views along a-axis (top) and c-axis (bottom) which both have 1-D channels through the axis and featured a **scu** topology. Color code: C - grey; O – red; Zr – cyan.

3.2 Metal Cation Incorporation via Post-synthetic Modification

To prepare the as-made Zr-tcpb-COOH for metal site incorporation, we carried out solvent exchange by immersing the sample in fresh MeOH, which was followed by treating with 0.01 M alkaline basic solution. The PXRD patterns of the base-treated samples remained unchanged (Figure 2b), indicating the integrity of the frameworks. Similar thermal stability was also observed for the samples after treatment (Figure 2c). We hypothesized that the acid-base neutralization will result in strong bonds between the metal cations and free carboxylic groups. The infrared (IR) spectroscopy was employed to examine and verify this hypothesis. as shown in Figure 2d, the IR spectrum of Zr-tcpb-COOH is dominated by the absorption bands associated with the vibrations of the organic linker, e.g., stretching modes $v_{as,s}$ of carboxylic group around 1600 and 1400 cm^{-}

^{1},[39] in plane/out of plane deformation modes $\delta_{ip,\ oop}$ of phenyl ring CH at 1018 and 867 cm^{-1}.[40, 41] Our previous studies have shown that the frequency of these modes is sensitive to its chemical environment.[41-43] The un-bonded carboxylic group of the H_4tcpb-$(COOH)_2$ linker is characterized by its featured bands *v*(C=O) at 1715 cm^{-1} and *v*(C-OH) at 1222 cm^{-1}. After the treatment in alkali hydroxide solution, most bands remained in the same positions except for *v*(C-OH) that shifted upward slightly to 1228 cm^{-1}. This further indicates that alkali/alkaline ions interact primarily with the -COOH moiety of the linkers. In addition, we notice the loss of the *v*(OH) band at 3670 cm^{-1}

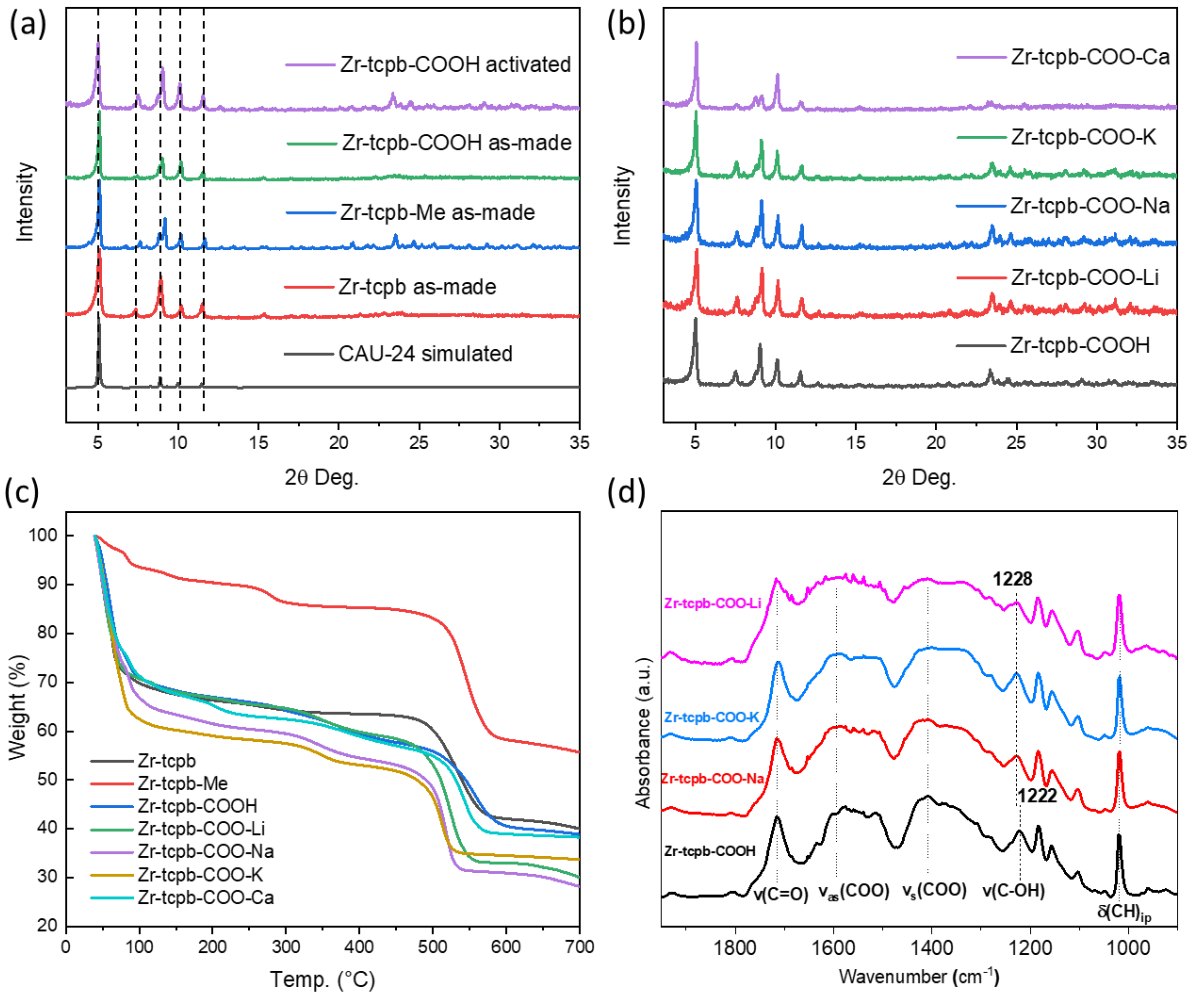

Figure 2. Powder X-ray diffraction patterns of isoreticular series of Zr-tcpb-X MOFs before (a) and after (b) treatment of alkali/alkaline aqueous solutions. The peaks match well with those of the simulated structure of CAU-24; (c) The thermogravimetric (TG) plots of the Zr-tcpb-X and Zr-tcpb-COOM series; (d) IR spectra of Zr-tcpb-COOH and samples after treating with alkali hydroxide solutions. All spectra are referenced to the blank KBr under vacuum. Notation and acronym: *v*, stretching; *δ*, deformation; *ip*, in plane; as, asymmetric; and s, symmetric.

that is attributed to the stretching mode of terminal and bridge -OH/H_2O on Zr_6O_4 clusters,[44] which suggests that hydroxide also reacted with these species (Figure S4). The presence of the characteristic peaks in the X-ray fluorescence (XRF) spectra (Figure S5) and X-ray photoelectron spectroscopy (XPS) plots (Figure S6) offers further evidence of the success of post-synthetic modification. The loading percentage was calculated to be 0.66 K and 0.71 Ca per ligand, respectively. The small difference in the conversion amount between the K and Ca samples is likely due to the longer treatment time and repeated treatment of the latter.

3.3 Gas Adsorption Analysis

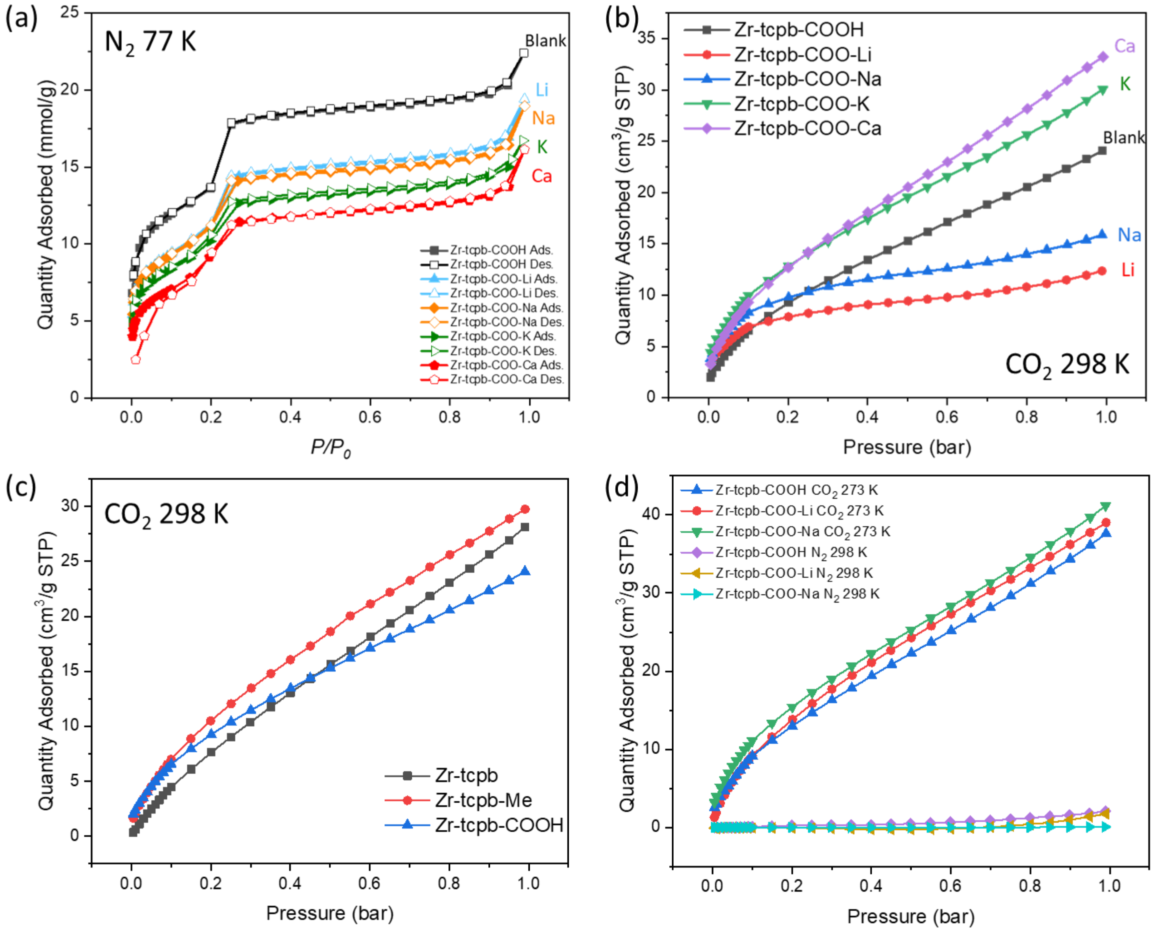

Figure 3. The gas adsorption-desorption isotherms of Zr-tcpb-COOM: (a) N_2 at 77 K and (b) CO_2 at 298 K; (c) The CO_2 adsorption isotherms of un-modified Zr-tcpb-X at 298 K; (d) Comparisons of adsorption isotherms of CO_2 and N_2 at 273 K and 298 K.

The permanent porosity of Zr-tcpb-COOM was evaluated using N_2 adsorption isotherm data collected at 77 K. The solvent-exchanged materials were activated at 373 K for 6 hours under high vacuum to remove the solvent molecules and coordinated water in the frameworks. All the N_2 isotherms show a two-step uptake indicating the presence of two types of pores (Figure 3a). Additionally, the quantity adsorbed decreased with the increase of atomic number which is reasonable since the molecular weight of sorbents increased accordingly. The estimated Brunauer-Emmett-Teller (BET) surface area values are 1075 m^2/g (Zr-tcpb-COOH), 837 m^2/g (Zr-tcpb-COOLi), 828 m^2/g (Zr-tcpb-COONa), 747 m^2/g (Zr-tcpb-COOK), and 632 m^2/g (Zr-tcpb-COOCa), respectively. The pore size distribution was calculated by the Horvath-Kawazoe model. The original 15 Å pore along the c-axis slightly shrunk owing to the occupancy of the larger metal cations (Figure S7).

Single component adsorption isotherms of carbon dioxide were measured at room temperature (298 K). The samples were activated under the same conditions as described earlier. It is interesting to note that CO_2 uptake capacity at 1 bar increases with the increasing atomic number (Li < Na < K < Ca), which is inverse to the trend of BET surface area. The uptake amounts for Zr-tcpb-COOCa is 33.22 cm^3/g STP (1.48 mmol/g) at 1 bar. Furthermore, all the cation modified samples demonstrated increases in uptake (increased by 66.5% at 0.05 bar in Zr-tcpb-COOK) within the low-pressure region (< 0.1 bar) when compared to the unmodified blank sample Zr-tcpb-COOH (Figure S8). This increase in uptake is attributed to the embedded metal sites that have stronger interactions with CO_2 compared to the free carboxylic acid. Additionally, all samples exhibit negligible uptake of N_2 at 298 K, indicating their excellent selectivity for CO_2 over N_2 (CO_2/N_2 IAST selectivity (15:85) = 539.5) (Figure 3d). The high selectivity of CO_2/N_2 may be attributed to the high affinity between the metal sites and CO_2 while such sites have very little interaction with N_2. Our compounds hold the highest CO_2/N_2 selectivity (0.15/0.85) among all Zr-based UiO-type MOFs, and the selectivity values are also among the highest when comparing to other stable MOFs such as MIL-101 and JLU-Liu45.[45-47] The dynamic adsorption of water was increased slightly due to the strong interaction of water and metals (Figure S9).

3.4 Solid-State NMR Analysis

The ^{13}C CP-MAS NMR spectra of the pristine and post-synthetically modified MOFs were taken (Figure 4a) and showed changes in the region associated with carboxylic acid groups (170-180 ppm) as a function of metal cation identity added to the material before activation (Figure 4c). Two overlapping resonances near 171 and 172 ppm are assigned to the four carboxylic acid groups on the linker that coordinate to the zirconium clusters, while carboxylic acid peaks above 174 ppm are assigned as belonging to the non-structural carboxylic acid group on the center benzene ring of the linker, which we will call the sidechain COOH. The ratio of integration of those two peaks in blank sample are 1.79 to 1, which matches with the ratio of different carboxylic acid groups on the building ligand. In the pristine material and in the monovalent cation-modified materials, a single peak is observed for this group, whereas for the Ca^{2+}-modified material, three peaks are observed. The sidechain COOH chemical shift increases from the pristine value when the material is post-synthetically modified with cations, suggesting an interaction between the cations and this sidechain COOH. The chemical shift of this group increases in a series from pristine < Na < Li < K < Ca, roughly following a trend down the periodic table with the exception of Na (Figure 4b and c). To better understand the environment around the metal cations, we performed ^{7}Li and ^{23}Na solid state NMR. The width and symmetry of peaks in NMR spectra of quadrupolar nuclei such as ^{23}Na or ^{7}Li are dependent on the symmetry of the electronic environment around the metal site. In the inactivated as-made materials, narrow resonances are observed in ^{7}Li and ^{23}Na spectra, corresponding to a symmetric environment of water ligands solvating the cations (Figure 4d and e). After activation, the ^{23}Na and ^{7}Li peaks broaden and shift up field slightly, suggesting a more asymmetric environment around the metal ions (Figure 4d and e). Peaks attributable to solvent and residual water are still present as observed by ^{13}C CP-

MAS and ^{1}H NMR (Figure S10), and the ^{13}C COOH peaks broaden inhomogeneously, suggesting a complex pore environment around the sidechain COOH groups in the activated materials comprised of cations and residual solvent molecules.

3.5 Recyclability and Chemical Stability

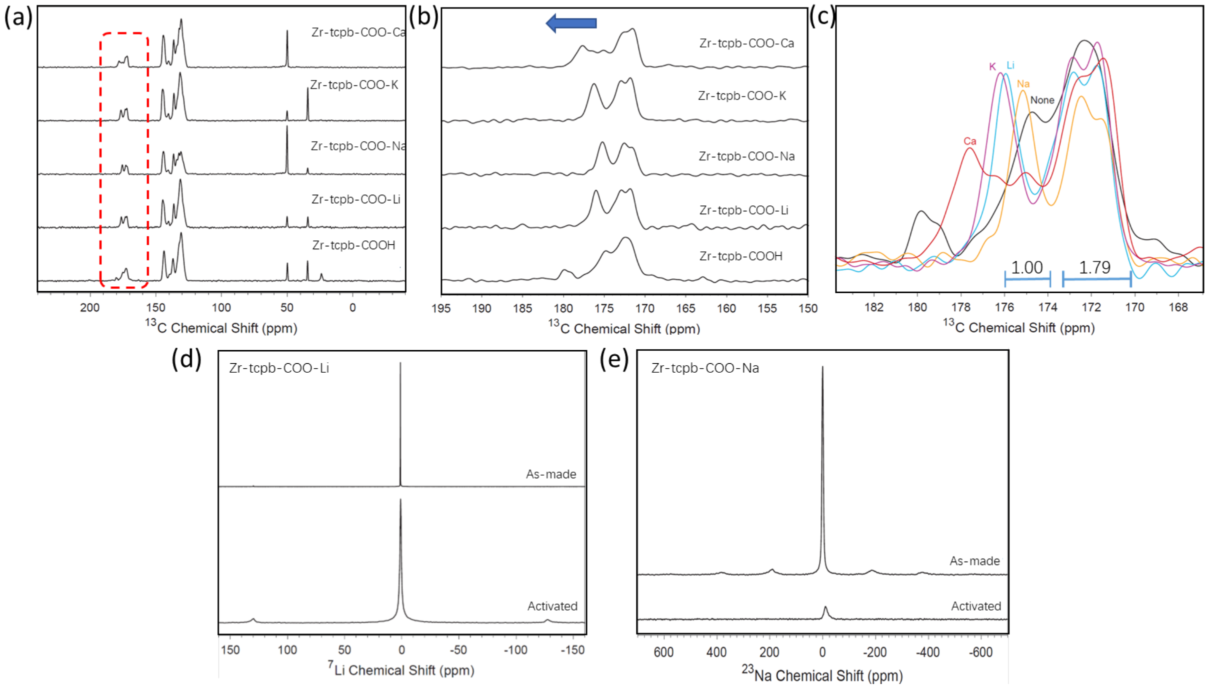

Figure 4. Solid-State ^{13}C CP-MAS NMR spectra of (a) as-made and modified samples; (b) carboxylic acid group region of as-made and modified samples; (c) overlap of carboxylic acid group region. ^{7}Li (d) and ^{23}Na (e) solid state NMR spectra of as-made and modified samples.

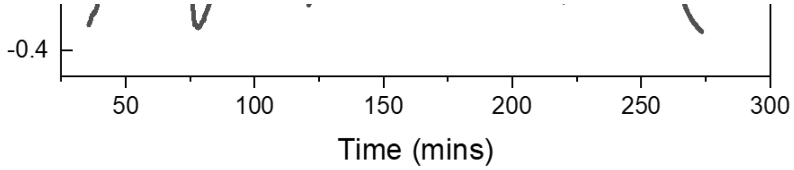

Figure 5. The CO_2 adsorption-desorption recyclability test results for the Zr-tcpb-COOCa sample. Five consecutive adsorption cycles were carried out with a gas feeding ratio CO_2: N_2 = 95:5 (v:v) at 303 K.

The recyclability of the MOF sorbents is a crucial evaluating factor that determines whether the materials have the potential for use in real-world industrial processes. To confirm the recyclability and stability of our compounds, we tested the samples with five consecutive CO_2 adsorption-desorption cycles. Zr-tcpb-COOCa was chosen for the recyclability measurements since it has the highest CO_2 uptake capacity. After activating the sample under 373 K in nitrogen flow, a CO_2: N_2 gas mixture with 95:5 ratio (v:v) was purged inside the sample chamber at 303 K (5% N_2 as balancing gas). The uptake amount of CO_2 was monitored by the weight change of the sample. As shown in Figure 5, the uptake capacity was found to be ~1.49 mmol/g, matching well with the single component adsorption data. More importantly, the uptake amount remains essentially constant for all five cycles, confirming the high stability and reusability of this sorbent.

Like the other zirconium MOFs with high connectivity, both Zr-tcpb-COOH and Zr-tcpb-COOM also demonstrate high resistance toward harsh conditions. For example, the as-made sample of Zr-tcpb-COOH remained highly crystalline after soaking in concentrated HCl and HNO_3 solution for 3 days and showed good stability in basic solution at low concentrations (up to 0.02M NaOH). The structure was intact even after 5 months of exposure in open air (Figure S3a). The Zr-tcpb-COOM samples also maintained high crystallinity in concentrated HCl and after the recyclability test (Figure S3b).

4. Conclusion

We have successfully designed and synthesized a series of isoreticular MOFs, Zr-tcpb-COOM, with alkali/alkaline earth metal cations introduced via post-synthetic modification. The creation of these metal sites leads to enhancement in carbon dioxide (CO_2) adsorption capacity, especially at very low CO_2 pressure. The increase in the CO_2 uptake capacity is in trend with the increase of cation's atomic number ($Li^+ < Na^+ < K^+ < Ca^{2+}$). Relatively high adsorption selectivity (CO_2/N_2 IAST selectivity (15:85) = 539.5) for carbon dioxide over nitrogen is achieved at room temperature. Zr-tcpb-COOCa reaches the highest capacity at 298 k and 1 bar among all Zr-tcpb-COOM. Moreover, the Zr-tcpb-COOM series exhibit high chemical stability, thermal stability, and excellent recyclability.

Associated Content

PXRD, XPS, NMR, XRF, etc. are available in the Supporting Information.

Author Information

Corresponding Author — Email: jingli@rutgers.edu (J.L.)

Notes — The authors declare no competing financial interest.

Author Contributions

G. Zhang: Methodology, Investigation, Formal analysis, Visualization, Writing – original draft. F. Xie: Investigation, Formal analysis. A. Patel: Investigation. T. Popp and A. Nieuwkoop: Investigation, Formal analysis. E. Morales and K. Tan: Investigation, Formal analysis. R. Crichton and J. Zhang: Investigation, Formal analysis. G. Hall: Formal analysis. J. Li: Conceptualization, Supervision, Validation, Writing – review & editing.

Conflicts of Interest

The authors declare no competing financial interest.

Acknowledgements

We are grateful for the financial support from the U.S. Department of Energy, Office of Science, Office of Basic Energy Sciences under Award No. DE-SC0019902.

References

1. E. S. Sanz-Pérez, C. R. Murdock, S. A. Didas and C. W. Jones, *Chemical Reviews*, 2016, **116**, 11840-11876.
2. X. Shi, H. Xiao, H. Azarabadi, J. Song, X. Wu, X. Chen and K. S. Lackner, 2020, **59**, 6984-7006.
3. L. Espinal, D. L. Poster, W. Wong-Ng, A. J. Allen and M. L. Green, *Environmental Science & Technology*, 2013, **47**, 11960-11975.
4. A. Samanta, A. Zhao, G. K. H. Shimizu, P. Sarkar and R. Gupta, *Industrial & Engineering Chemistry Research*, 2012, **51**, 1438-1463.
5. S. Xiang, Y. He, Z. Zhang, H. Wu, W. Zhou, R. Krishna and B. Chen, *Nature Communications*, 2012, **3**, 954.
6. H. Lyu, O. I.-F. Chen, N. Hanikel, M. I. Hossain, R. W. Flaig, X. Pei, A. Amin, M. D. Doherty, R. K. Impastato, T. G. Glover, D. R. Moore and O. M. Yaghi, *Journal of the American Chemical Society*, 2022, **144**, 2387-2396.
7. H. Mao, J. Tang, G. S. Day, Y. Peng, H. Wang, X. Xiao, Y. Yang, Y. Jiang, S. Chen, D. M. Halat, A. Lund, X. Lv, W. Zhang, C. Yang, Z. Lin, H.-C. Zhou, A. Pines, Y. Cui and J. A. Reimer, 2022, **8**, eabo6849.
8. J. Wang, L. Huang, R. Yang, Z. Zhang, J. Wu, Y. Gao, Q. Wang, D. O'Hare and Z. Zhong, *Energy & Environmental Science*, 2014, **7**, 3478-3518.
9. M. Ding, R. W. Flaig, H.-L. Jiang and O. M. Yaghi, *Chemical Society Reviews*, 2019, **48**, 2783-2828.
10. Z. Hu, Y. Wang, B. B. Shah and D. Zhao, 2019, **3**, 1800080.
11. J.-B. Lin, T. T. T. Nguyen, R. Vaidhyanathan, J. Burner, J. M. Taylor, H. Durekova, F. Akhtar, R. K. Mah, O. Ghaffari-Nik, S. Marx, N. Fylstra, S. S. Iremonger, K. W.

Dawson, P. Sarkar, P. Hovington, A. Rajendran, T. K. Woo and G. K. H. Shimizu, 2021, **374**, 1464-1469.

12. H. Wu, R. S. Reali, D. A. Smith, M. C. Trachtenberg and J. Li, 2010, **16**, 13951-13954.
13. J. Cure, E. Mattson, K. Cocq, H. Assi, S. Jensen, K. Tan, M. Catalano, S. Yuan, H. Wang, L. Feng, P. Zhang, S. Kwon, J.-F. Veyan, Y. Cabrera, G. Zhang, J. Li, M. Kim, H.-C. Zhou, Y. J. Chabal and T. Thonhauser, *Journal of Materials Chemistry A*, 2019, **7**, 17536-17546.
14. M. Jahandar Lashaki, S. Khiavi and A. Sayari, *Chemical Society Reviews*, 2019, **48**, 3320-3405.
15. J. H. Choe, H. Kim, M. Kang, H. Yun, S. Y. Kim, S. M. Lee and C. S. Hong, *Journal of the American Chemical Society*, 2022, **144**, 10309-10319.
16. B. Dinakar, A. C. Forse, H. Z. H. Jiang, Z. Zhu, J.-H. Lee, E. J. Kim, S. T. Parker, C. J. Pollak, R. L. Siegelman, P. J. Milner, J. A. Reimer and J. R. Long, *Journal of the American Chemical Society*, 2021, **143**, 15258-15270.
17. T. M. McDonald, J. A. Mason, X. Kong, E. D. Bloch, D. Gygi, A. Dani, V. Crocellà, F. Giordanino, S. O. Odoh, W. S. Drisdell, B. Vlaisavljevich, A. L. Dzubak, R. Poloni, S. K. Schnell, N. Planas, K. Lee, T. Pascal, L. F. Wan, D. Prendergast, J. B. Neaton, B. Smit, J. B. Kortright, L. Gagliardi, S. Bordiga, J. A. Reimer and J. R. Long, *Nature*, 2015, **519**, 303-308.
18. R. W. Flaig, T. M. Osborn Popp, A. M. Fracaroli, E. A. Kapustin, M. J. Kalmutzki, R. M. Altamimi, F. Fathieh, J. A. Reimer and O. M. Yaghi, *Journal of the American Chemical Society*, 2017, **139**, 12125-12128.
19. C. E. Bien, K. K. Chen, S.-C. Chien, B. R. Reiner, L.-C. Lin, C. R. Wade and W. S. W. Ho, *Journal of the American Chemical Society*, 2018, **140**, 12662-12666.
20. C. E. Bien, Q. Liu and C. R. Wade, *Chemistry of Materials*, 2020, **32**, 489-497.
21. Z. Cai, C. E. Bien, Q. Liu and C. R. Wade, *Chemistry of Materials*, 2020, **32**, 4257-4264.
22. H. Wang, J. Peng and J. Li, 2016, **16**, 1298-1310.
23. A. Torrisi, R. G. Bell and C. Mellot-Draznieks, *Crystal Growth & Design*, 2010, **10**, 2839-2841.
24. H. Huang, W. Zhang, F. Yang, B. Wang, Q. Yang, Y. Xie, C. Zhong and J.-R. Li, *Chemical Engineering Journal*, 2016, **289**, 247-253.
25. N. Li, Z. Chang, H. Huang, R. Feng, W.-W. He, M. Zhong, D. G. Madden, M. J. Zaworotko and X.-H. Bu, 2019, **15**, 1900426.
26. A. L. Dzubak, L.-C. Lin, J. Kim, J. A. Swisher, R. Poloni, S. N. Maximoff, B. Smit and L. Gagliardi, *Nature Chemistry*, 2012, **4**, 810-816.
27. X. Kong, E. Scott, W. Ding, J. A. Mason, J. R. Long and J. A. Reimer, *Journal of the American Chemical Society*, 2012, **134**, 14341-14344.
28. B. Liu, S. Yao, X. Liu, X. Li, R. Krishna, G. Li, Q. Huo and Y. Liu, *ACS Applied Materials & Interfaces*, 2017, **9**, 32820-32828.
29. M. Jia, J. Li, J. Gu, L. Zhang and Y. Liu, *Materials Chemistry Frontiers*, 2021, **5**, 1398-1404.
30. H. A. Evans, D. Mullangi, Z. Deng, Y. Wang, S. B. Peh, F. Wei, J. Wang, C. M. Brown, D. Zhao, P. Canepa and A. K. Cheetham, *Science Advances*, 2022, **8**, eade1473.
31. J. S. Choi, J. Bae, E. J. Lee and N. C. Jeong, *Inorganic Chemistry*, 2018, **57**, 5225-5231.
32. A. Ö. Yazaydın, A. I. Benin, S. A. Faheem, P. Jakubczak, J. J. Low, R. R. Willis and R. Q. Snurr, *Chemistry of Materials*, 2009, **21**, 1425-1430.

33. E. D. Bloch, D. Britt, C. Lee, C. J. Doonan, F. J. Uribe-Romo, H. Furukawa, J. R. Long and O. M. Yaghi, *Journal of the American Chemical Society*, 2010, **132**, 14382-14384.
34. S. Shang, C. Yang, M. Sun, Z. Tao, A. Hanif, Q. Gu and J. Shang, *Separation and Purification Technology*, 2022, **301**, 122058.
35. S. J. Datta, C. Khumnoon, Z. H. Lee, W. K. Moon, S. Docao, T. H. Nguyen, I. C. Hwang, D. Moon, P. Oleynikov, O. Terasaki and K. B. Yoon, *Science*, 2015, **350**, 302-306.
36. M. Lammert, H. Reinsch, C. A. Murray, M. T. Wharmby, H. Terraschke and N. Stock, *Dalton Transactions*, 2016, **45**, 18822-18826.
37. Z. Chen, S. L. Hanna, L. R. Redfern, D. Alezi, T. Islamoglu and O. K. Farha, *Coordination Chemistry Reviews*, 2019, **386**, 32-49.
38. G. Zhang, K. Tan, S. Xian, K. Xing, H. Sun, G. Hall, L. Li and J. Li, *Inorganic Chemistry*, 2021, **60**, 11730-11738.
39. K. I. Hadjiivanov, D. A. Panayotov, M. Y. Mihaylov, E. Z. Ivanova, K. K. Chakarova, S. M. Andonova and N. L. Drenchev, *Chemical Reviews*, 2021, **121**, 1286-1424.
40. E. Velasco, Y. Osumi, S. J. Teat, S. Jensen, K. Tan, T. Thonhauser and J. Li, *Chemistry*, 2021, **3**, 327-337.
41. K. Tan, N. Nijem, P. Canepa, Q. Gong, J. Li, T. Thonhauser and Y. J. Chabal, *Chemistry of Materials*, 2012, **24**, 3153-3167.
42. H.-Q. Yin, K. Tan, S. Jensen, S. J. Teat, S. Ullah, X. Hei, E. Velasco, K. Oyekan, N. Meyer, X.-Y. Wang, T. Thonhauser, X.-B. Yin and J. Li, *Chemical Science*, 2021, **12**, 14189-14197.
43. K. Tan, S. Zuluaga, Q. Gong, P. Canepa, H. Wang, J. Li, Y. J. Chabal and T. Thonhauser, *Chemistry of Materials*, 2014, **26**, 6886-6895.
44. N. Planas, J. E. Mondloch, S. Tussupbayev, J. Borycz, L. Gagliardi, J. T. Hupp, O. K. Farha and C. J. Cramer, *The Journal of Physical Chemistry Letters*, 2014, **5**, 3716-3723.
45. X. Sun, X. Li, S. Yao, R. Krishna, J. Gu, G. Li and Y. Liu, *Journal of Materials Chemistry A*, 2020, **8**, 17106-17112.
46. W. Zhang, H. Huang, C. Zhong and D. Liu, *Physical Chemistry Chemical Physics*, 2012, **14**, 2317-2325.
47. K. Munusamy, G. Sethia, D. V. Patil, P. B. Somayajulu Rallapalli, R. S. Somani and H. C. Bajaj, *Chemical Engineering Journal*, 2012, **195-196**, 359-368.